Dalton Transactions

PAPER

View Article Online
View Journal | View Issue

Cite this: *Dalton Trans.*, 2014, **43**, 7998

Controlled synthesis of Au–Fe_3O_4 hybrid hollow spheres with excellent SERS activity and catalytic properties†

Qian Gao,[a,b] Aiwu Zhao,*[a,b] Hongyan Guo,[a] Xucheng Chen,[a] Zibao Gan,[a] Wenyu Tao,[a] Maofeng Zhang,[a] Rong Wu[a] and Zhenxin Li[a]

Received 29th January 2014,
Accepted 11th March 2014

DOI: 10.1039/c4dt00312h

www.rsc.org/dalton

Au–Fe_3O_4 hybrid hollow spheres have been successfully synthesized by a one-pot process *via* the hydrothermal treatment of $FeCl_3$, $HAuCl_4$, citrate, urea, and polyacrylamide (PAM). The amount of Au nanoparticles located in the hybrid hollow spheres can be tuned by changing the molar ratio of Au/Fe precursors. A possible synthetic mechanism of the Au–Fe_3O_4 hybrid hollow spheres has been proposed. The obtained hybrids exhibit not only a superior surface-enhanced Raman scattering (SERS) sensitivity, but also an excellent catalytic activity. The detection limit of the Au–Fe_3O_4 hybrid hollow spheres (the Au/Fe molar ratio is 0.2, Au–Fe_3O_4-0.2) for R6G can reach up to 10^{-10} M, which can meet the required concentration level for ultratrace detection of analytes using SERS. Furthermore, the catalytic experiments of the Au–Fe_3O_4-0.2 hybrid hollow spheres demonstrate that the model of 4-nitrophenol (4-NP) molecules can be degraded within 3 min and the catalytic activity can be recovered without sharp activity loss in six runs, which indicates their superior catalytic degradation activity. The reason may be due to the highly efficient partial charge transfer between Au and Fe_3O_4 at the nanoscale interface. The results indicate that the bifunctional Au–Fe_3O_4 hybrid hollow spheres can serve as promising materials in trace detection and industrial waste water treatment.

1. Introduction

Assembling several materials into a single nanoparticle with tunable composition, size, and morphology is a promising strategy for achieving novel properties with applications in diverse areas such as optics,[1] magnetics,[2] catalysts,[3] chemical sensors,[4] biomedical applications[5] and so on. To date, significant advances in the controlled synthesis of composite nanoparticles have been made.[6] As one of the hybrid nanomaterials, gold–iron oxide nanocomposites (Au–Fe_3O_4) have been particularly attractive to researchers recently due to their combined optical, catalytic, and magnetic properties.[7–12] Metal oxide deposition on noble metals is known to affect their optical properties, *e.g.*, the plasmon resonance frequency is shifted.[13,14] From this viewpoint, composite structures comprising of nanometric iron oxide particles and gold nanoparticles have significant potential.

Nowadays, a number of procedures have been reported for preparing such Au–Fe_3O_4 hybrid nanoparticles.[5,13–29] For example, Sun and co-workers[16] have reported the synthesis of dumbbell-like Au–Fe_3O_4 nanoparticles using decomposition of $Fe(CO)_5$ on the surface of pre-formed Au particles, followed by oxidation in 1-octadecene. Fe_3O_4–Au core–shell nanoparticles could be prepared with room-temperature coating of Au on the surface of Fe_3O_4 nanoparticles by reducing $HAuCl_4$ in a chloroform solution of oleylamine.[5] Guo *et al.*[18] have synthesized diverse noble-metal/Fe_3O_4, TiO_2, and carbon nanotube hybrids using 3-aminopropyltrimethoxysilane (APTMS) as a linker, and found that the hybrid materials exhibited superior electrochemical properties. Liu *et al.*[26] have used a two-step nanoemulsion process to synthesize Au–Fe_3O_4 hybrid core–shell nanoparticles in one pot by using nontoxic precursors. They found that the structural arrangement enhanced the magnetic and optical functionalities beyond those of the individual components. However, these methods mentioned above either need toxic and expensive reagents or surfactants such as oleylamine and $Fe(CO)_5$, or require multiple steps which are often accompanied by some disadvantages such as low efficiency and tedious processing steps. On the other hand, hollow

[a]*Institute of Intelligent Machines, Chinese Academy of Sciences, Hefei, 230031, P. R. China*
[b]*State Key Laboratory of Transducer Technology, Chinese Academy of Sciences, Hefei, 230031, P. R. China. E-mail: awzhao@iim.ac.cn; Fax: +86-551-65592420; Tel: +86-551-65593360*

†Electronic supplementary information (ESI) available. See DOI: 10.1039/c4dt00312h

metallic nanostructures, in addition to advantages of high specific surface, low density, saving of material and reduction of cost, are exceptionally promising materials due to their intriguing surface plasmonic properties and catalytic activities different from their solid counterparts. However, to the best of our knowledge, there have been few reports on the synthesis of hollow Au–Fe_3O_4 hybrid spheres. Thus, it is highly attractive and of great significance to develop a facile, reliable, inexpensive, and controllable strategy to fabricate Au–Fe_3O_4 hollow spheres by using a nontoxic solvent and reagents under mild conditions and to explore their potential applications from both scientific and applicability perspectives.

Herein, we present a simple one-pot method for the synthesis of Au–Fe_3O_4 hollow nanocomposites based on the hydrothermal treatment of $FeCl_3{\cdot}6H_2O$, $HAuCl_4$, citrate, polyacrylamide (PAM), and urea. The weight ratio of the Au nanoparticles located in the hybrid particles can be controlled by varying the concentration of the precursors. Owing to the less expensive and nontoxic raw reaction materials, especially water as the solvent, our method represents an economical and green approach for the controlled synthesis of Au–Fe_3O_4 hybrid hollow spheres. The as-prepared Au–Fe_3O_4 hollow hybrids exhibit pronounced surface-enhanced Raman scattering (SERS) activity, which may possibly be used as an optical probe with magnetic function for application in high-sensitivity bioassays. Meanwhile, they have excellent catalytic activity for the reduction of 4-nitrophenol (4-NP) in the presence of $NaBH_4$. More importantly, the obtained hollow hybrids exhibit high water solubility and magnetic properties with relatively high saturation magnetization at room temperature, which are of special importance in potential applications.

2. Experimental section

2.1. Synthesis of Au–Fe_3O_4 hybrid hollow spheres

Au–Fe_3O_4 hybrid hollow spheres were prepared by the one-pot hydrothermal method. All of the chemical reagents were of analytical grade and used without further purification. In a typical synthesis, 0.45 mmol of $FeCl_3{\cdot}6H_2O$, 1.2 mmol of sodium citrate ($C_6H_5O_7Na_3{\cdot}2H_2O$), 1.8 mmol of urea, and 0.09 g of PAM were dissolved in distilled water. Then, a certain amount of $HAuCl_4$ was added under vigorous stirring until it was totally dissolved. The total volume of the reaction solution is about 12 mL. After an hour, the solution was transferred to a 15 mL Teflon-lined stainless-steel autoclave. The autoclave was then sealed and maintained at 200 °C for 12 h. After the autoclave had cooled down to room temperature naturally, the black products were separated magnetically. The obtained sediments were washed with distilled water and absolute ethanol several times, and then dried in a vacuum desiccation oven at 60 °C overnight. In this synthesis, the final products which are synthesized under different Au/Fe molar ratios of 0, 0.05, 0.1, 0.2 and 0.5 are defined as Au–Fe_3O_4-0, Au–Fe_3O_4-0.05, Au–Fe_3O_4-0.1, Au–Fe_3O_4-0.2, and Au–Fe_3O_4-0.5, respectively.

2.2. SERS measurements

Rhodamine 6G (R6G) dye was used as Raman probes for the SERS sensitivity of the Au–Fe_3O_4 hybrid hollow spheres. Typically, an aqueous solution of Au–Fe_3O_4 hybrid hollow spheres with different Au/Fe molar ratios (20 μL) was added dropwise onto a glass substrate and dried under ambient conditions, and then a 1×10^{-5} M ethanolic solution (20 μL) of R6G was added dropwise onto the resulting nanostructure film and allowed to dry. After washing the substrate with ethanol and drying under N_2, SERS spectra were recorded under ambient conditions.

2.3. Catalytic properties

The reduction of the 4-NP compound by the water-soluble Au–Fe_3O_4 hybrid hollow spheres in the presence of $NaBH_4$ was carried out to examine the catalytic activity and recyclability of the Au–Fe_3O_4 hybrid hollow spheres. 2.1 mL of deionized water, 0.15 mL of 1×10^{-3} M 4-NP, and 0.75 mL of 0.1 M $NaBH_4$ solutions were added into a quartz cuvette followed by addition of 2 mg of water-soluble Au–Fe_3O_4 hollow spheres to the mixture. The color of the mixture gradually changed from yellow to colorless. During the reaction, a quantitative portion of the mixture was taken at regular intervals and analyzed by UV-vis spectroscopy. For the recycling experiment, the catalysts were collected using an external magnetic field, washed two times with deionized water, and then reused for the reduction of 4-NP repeatedly.

2.4. Characterization

The phase and composition of the products were determined using a Rigaku D/Max-gA rotating-anode X-ray diffractometer with monochromatic high-intensity Cu-Kα radiation (λ = 1.54187 Å). The morphologies and structures of the products were observed with field emission scanning electron microscopy (FESEM, Quanta-200, FEI, USA). Transmission electron microscopy (TEM) and energy dispersive spectroscopy (EDS) studies were conducted on a JEM-2010 microscope with an energy dispersive X-ray detector. UV-vis absorption spectra of the products were recorded with a Shimadzu DUV-3700 UV-vis spectrophotometer. Specific surface areas were calculated using the Brunauer–Emmett–Teller (BET, Ommishop 100 cx) model, and the pore size distributions were evaluated from the desorption branches of the nitrogen isotherms using the Barrett–Joyner–Halenda (BJH) model. Magnetic properties of the products were measured on a superconducting quantum interference device (SQUID) magnetometer at room temperature. Raman measurements were conducted on a confocal microscopy DXR Smart-Raman Spectrometer (Thermo Scientific) equipped with a CCD detector and a holographic notch filter. Radiation of 532 nm from an air–argon ion laser (Spectra-Physics model 163-C4260) was used for excitation. The laser beam was focused on a sample of about 2 μm in size. The acquisition time was 2 s for each spectrum. For each substrate, we took three SERS spectra in different positions of the substrate and then averaged them.

3. Results and discussion

3.1. Synthesis and characterization of Au–Fe_3O_4 hybrid hollow spheres

The essence of our one-pot methodology is based on a solvothermal route, which involves a preliminary Au formation stage, a complete hybrid stage, and an Ostwald ripening stage. Scheme 1 shows the synthetic procedure of the Au–Fe_3O_4 hybrid hollow spheres. The homogeneous synthesis solution contains Au precursor, Fe_3O_4 precursor, PAM, urea, and trisodium citrate in H_2O. According to previous reports, at elevated temperatures, citrate or citrate acid can serve as a reductant in solution due to its hydroxyl group.[30] The metallic ions are very easy to reduce to form noble nanoparticles under the high temperature reaction, so the Au nanoparticles can be formed first during the stage. The Au nanoparticles are covered by the existing $C_6H_5O_7^{3-}$, which are available for stabilizing the particles and preventing the small particles from aggregating into bigger ones. Due to the electrostatic interaction between the $C_6H_5O_7^{3-}$ and Fe^{3+}, sorption of Fe^{3+} on the Au NPs surface occurs. With the increase of the reaction time, then into a hybrid stage, part of the Fe^{3+} ions will be reduced to Fe^{2+} by citrate. At the same time, urea decomposes into NH_3 and CO_2, which provides an alkaline atmosphere for the solution system. The alkaline conditions lead to the formation of $Fe(OH)_3$ and $Fe(OH)_2$ which will be transformed into Fe_3O_4 after dehydration. Due to the strong metal–oxide interaction at the interface, heterogeneous nucleation of Fe_3O_4 on the Au NPs takes relative priority over self-nucleation in the solution. Afterwards, the newly formed amorphous particles aggregate into round spheres, driven by minimization of the total surface energy. In this stage, the cooperative influences of citrate and PAM are critical for the formation of monodisperse hybrid spheres. Their roles are interpreted as follows. For citrate, aside from its reducing properties, it is also a chelating ligand with strong coordinating ability, which can coordinate with Au and iron ions (Fe^{3+} or Fe^{2+}) to form stable complexes.[31] The formation of complexes can sharply reduce the availability of free iron ions in aqueous solution, resulting in a slow reaction rate which is crucial for the formation of well dispersed spherical products. The polymer PAM plays two roles in this synthesis system. On the one hand, PAM can work as a capping agent for the stabilizer.[32] Due to the large amount of amide ligands, PAM can be absorbed on the surface of the product, consequently stabilizing the primary particles. On the other hand, with the introduction of PAM, the viscosity of the solution becomes greater. The increased viscosity will slow down the reaction rate as well as the movement rate of primary nanoparticles,[33] which can allow primary nanoparticles to have enough time to aggregate into regular round spheres. Finally, with the further increase of the reaction time, the well known Ostwald ripening process and the gaseous cavities formed by the decomposition of less urea dominate the morphological evolution of hollow spheres.

Fig. 1 gives a series of X-ray diffraction (XRD) patterns of the Au–Fe_3O_4 hybrid hollow spheres with various Au/Fe molar ratios. When no $HAuCl_4$ was added to the starting solution, only pure Fe_3O_4 hollow spheres were obtained as the final product (Fig. 1a). Six major reflections appearing in curve a located at about 30.4°, 35.4°, 43.2°, 53.4°, 57.2°, and 62.7° can be assigned to diffraction of the Fe_3O_4 crystal with an inverse spinel structure from the (220), (311), (400), (422), (511), and (440) (JCPDS card no. 01-1111), respectively. No other peaks were observed in curve a, indicating that the spheres are in pure Fe_3O_4 crystalline phase. With the increase of the amount of $HAuCl_4$, there are other diffraction peaks at 38.1°, 44.3°, 64.6° and 77.5° present in curves b–e, which correspond to the

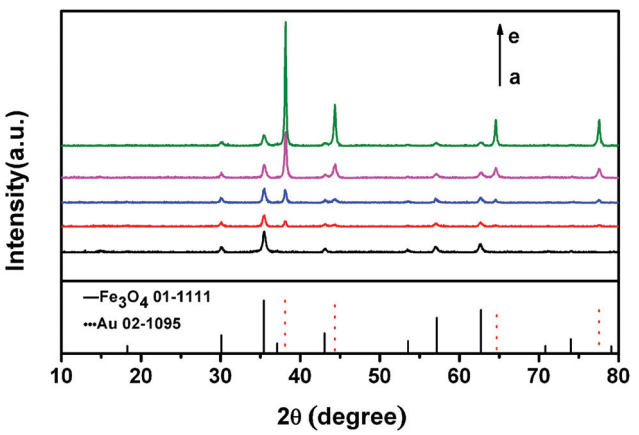

Fig. 1 XRD patterns of the Au–Fe_3O_4 hybrid hollow spheres with various Au/Fe molar ratios: (a) Au–Fe_3O_4-0, (b) Au–Fe_3O_4-0.05, (c) Au–Fe_3O_4-0.1, (d) Au–Fe_3O_4-0.2 and (e) Au–Fe_3O_4-0.5.

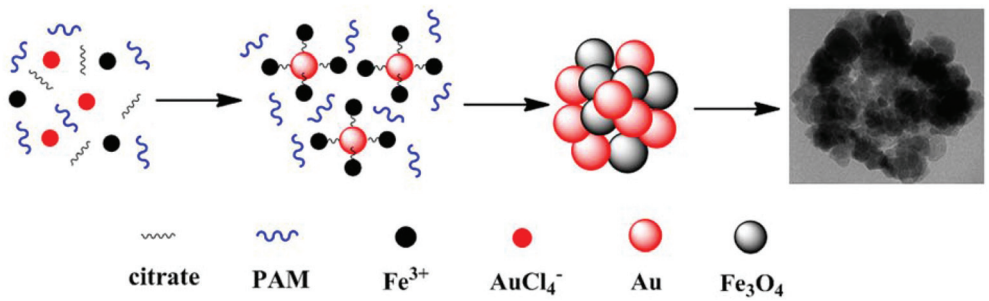

Scheme 1 The formation process of the Au–Fe_3O_4 hybrid hollow spheres.

(111), (200), (220) and (311) planes of the gold crystal with a cubic phase (JCPDS card no. 02-1095).[34] The evolution of the diffraction peaks from fcc Au is clearly seen in the patterns. As the Au proportion increases, the diffraction from Au dominates the patterns, and the diffraction from Fe_3O_4 becomes weak due to the heavy atom effect of Au.[13] This result further proved that the Au to Fe weight ratio in the particle can be controlled in the synthesis.

The morphology and structure of the as-synthesized products were investigated by transmission electron microscopy (TEM) and field emission scanning electron microscopy (FESEM), respectively. Representative images of the typical sample of Au–Fe_3O_4-0.2 are shown in Fig. 2. A panoramic view reveals that the as-prepared products consist of uniform spherical particles without any impurities (Fig. 2a), and the average size of the microspheres is approximately 200 nm. In the high magnification SEM image (Fig. 2b), a great number of cracks on the surface of the spheres can be clearly observed, indicating the porous structure of the spheres. From the typical TEM image (Fig. 2c), we can observe that the spheres have a pale center region in contrast to a dark edge, suggesting that the spheres are hollow. The shell thickness is about 40 nm and the surface is relatively rough, which indicate that the shell is composed of irregular shaped tiny primary nanocrystals. Surprisingly, there are some small black dots (20 nm) randomly distributed in the shell of the hollow sphere, which suggests that the as-prepared microspheres are composed of Au and Fe_3O_4 two components. To further determine the composition of the samples, energy dispersive spectroscopy (EDS) was performed on an individual composite particle. The spectrum in Fig. 2d indicates the presence of Fe, Au, and O elements, proving the formation of Fe_3O_4 and Au. The signals of Cu, Cr, and C in the EDS spectrum originate from the carbon-coated copper grid. In this analysis, no Au signal is found when the EDS are focused on the surface of the Fe_3O_4 shell region (Fig. 2e). Therefore, it is believed that the Au and Fe_3O_4 primary particles in the hollow spheres are randomly distributed.

The weight ratio of the Au nanoparticles located in the hollow spheres can be controlled by varying the Au/Fe molar ratios of the precursors present in the reaction mixture. When no $HAuCl_4$ was added to the starting solution, only pure Fe_3O_4 hollow spheres were obtained (Fig. 1a and Fig. S1†) (defined as Au–Fe_3O_4-0). When the Au/Fe molar ratio increases to 0.05, only a few black dots are observed on the shell of the hollow spheres (Fig. S2b†) and the product consists of well dispersed spheres with a coarse surface (defined as Au–Fe_3O_4-0.05, Fig. S2a†). Fig. S3† shows SEM and TEM images of the Au–Fe_3O_4 composites which were prepared with a 0.1 Au/Fe molar ratio. In this case, the black dots appearing in the hollow spheres increase and the particles also increase with a coarse surface (defined as Au–Fe_3O_4-0.1). With an increase of the Au/Fe molar ratio (0.2), the number of Au domains in the hollow sphere increases (Fig. 1d and 2c, defined as Au–Fe_3O_4-0.2). With a further increase of the Au/Fe molar ratio to 0.5, more Au nanoparticles are found and aggregate to form large black dots in the hollow sphere (defined as Au–Fe_3O_4-0.5, Fig. S4b†). Unfortunately, some of them grow out of the hollow spheres (Fig. S4a and c†). Moreover, it is also noticeable that with the increase of the weight ratio of Au nanoparticles, the products

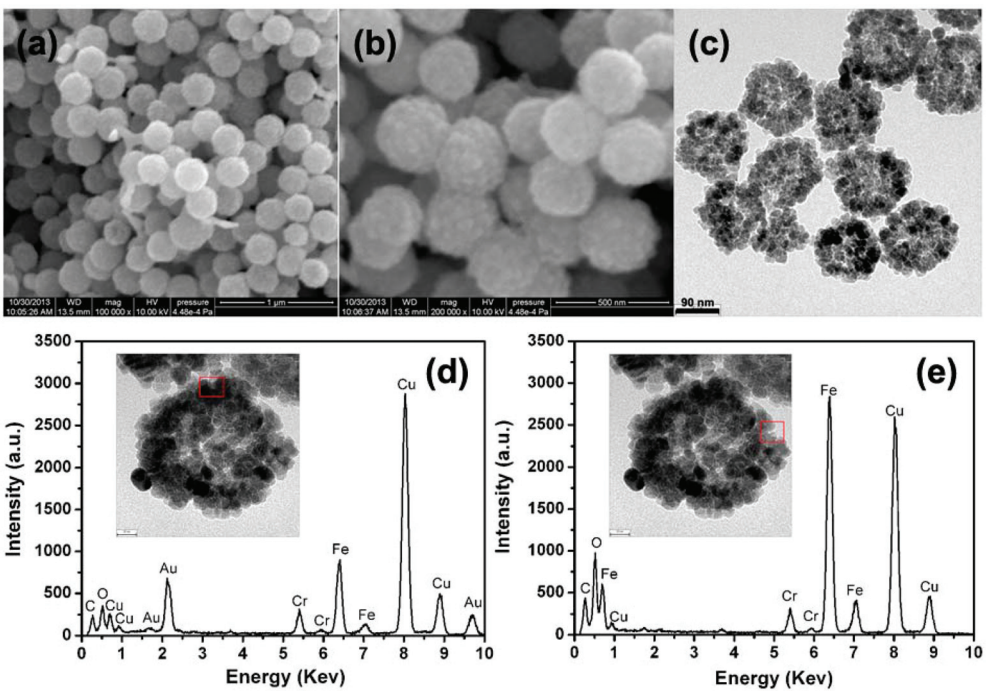

Fig. 2 SEM, TEM and EDS data of the Au–Fe_3O_4-0.2 hybrid hollow spheres: (a, b) SEM images, (c) TEM images and (d, e) EDS data taken from different areas of the shell.

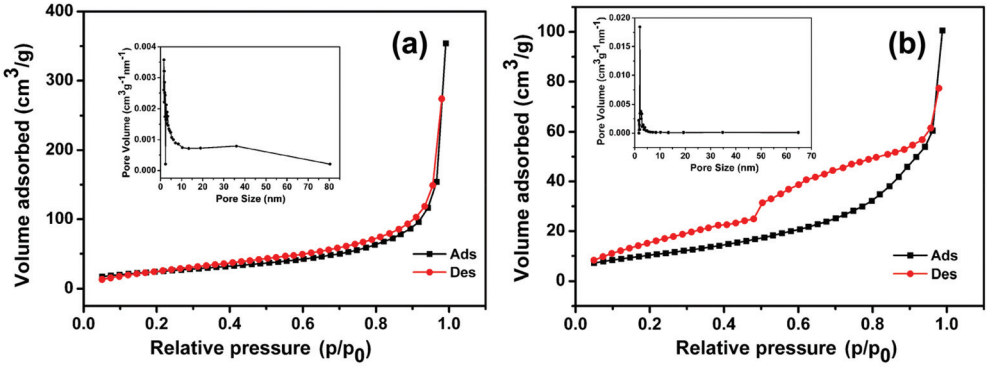

Fig. 3 N_2 adsorption–desorption isotherms and BJH pore plots (inset) of the samples: (a) Au–Fe_3O_4-0 and (b) Au–Fe_3O_4-0.5.

will be transformed from a highly porous structure into a relatively dense structure with a smooth surface.

This change can be substantiated by the measurement of nitrogen adsorption–desorption isotherms and the Brunauer–Emmett–Teller (BET) surface area (Fig. 3). According to the IUPAC classification,[35] the isotherms could be categorized as type IV with an inconspicuous hysteresis loop observed in the range of 0.4–1.0P/P_0 for the sample Au–Fe_3O_4-0 and 0.05–0.95P/P_0 for the sample Au–Fe_3O_4-0.5, indicating the presence of mesopores. The BET surface areas of the two hollow spheres are 88.477 and 38.832 $m^2\ g^{-1}$, respectively, which are much larger than the value for single crystal magnetite hollow spheres reported in the literature (13.5 $m^2\ g^{-1}$).[36] BJH calculations for the pore size distribution (insets in Fig. 3a and 3b) revealed that the distributions for the two samples are centered at approximately 1.6 and 2.0 nm, respectively. The mesopores on the two hollow spheres can be attributed to the interspaces of the constituent particles. In addition, it is clearly observed that with the increase of the weight ratio of Au nanoparticles located in the hollow spheres, the value of the surface area decreases to 38.832 $m^2\ g^{-1}$ (Fig. 3b). This result also reveals that an appropriate Au/Fe molar ratio is critical for the formation of the desired hollow hybrid spheres.

The magnetic properties of representative samples of Au–Fe_3O_4-0 and Au–Fe_3O_4-0.5 hybrid hollow spheres were characterized using a SQUID magnetometer at room temperature in the applied field sweeping from −10 to 10 kOe (Fig. 4). The specific saturated magnetizations (M_s) are 72.9 and 42 emu g^{-1} for Au–Fe_3O_4-0 and Au–Fe_3O_4-0.5 hybrid hollow spheres, respectively. The decrease in M_s for the hollow hybrid spheres is mainly due to the introduction of gold.[37] On the basis of the data for near zero magnetization, the coercivity shows (insets in Fig. 4) a clear increase for Au–Fe_3O_4 hollow hybrid spheres (3 Oe for Au–Fe_3O_4-0 and 11 Oe for Au–Fe_3O_4-0.5), reflecting the fact that coercivity of a superparamagnetic nanoparticle is related to a change in dipolar coupling or a change in the magnetic particle size.[38] The increase in coercivity can be attributed to the increase of the Au weight ratio in the hollow hybrids, which leads to a less-effective coupling of the magnetic dipole moments. Moreover, the suspensions of the Au–Fe_3O_4-0.5 hybrid hollow spheres can be concentrated on

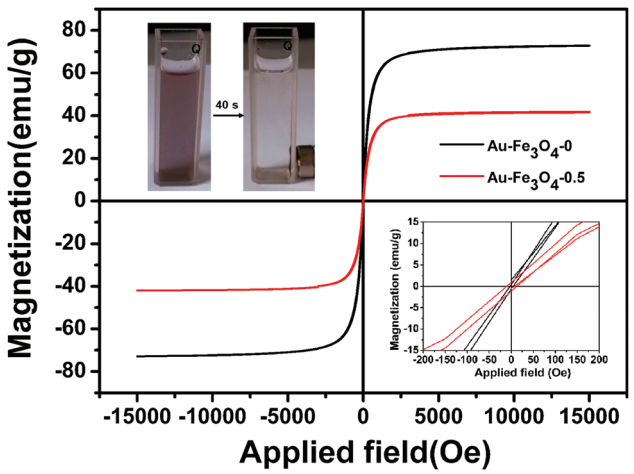

Fig. 4 Magnetic hysteresis loops of the Au–Fe_3O_4-0 and Au–Fe_3O_4-0.5 hybrid hollow spheres (the insets show their suspensions before and after magnetic separation by an external magnet and the magnified low field curves, respectively).

the side of the quartz cell by an external magnet within 40 s (see the insets in Fig. 4), leaving the aqueous solution transparent. After removing the magnet, the magnetite particles will be redispersed in the aqueous solution by shaking. This excellent water-dispersive ability and magnetic response allow for the tracking or separation of such particles in a magnetic gradient, paving the way for their sensitive detection and recycling in practical applications.

3.2. SERS performance of the Au–Fe_3O_4 hybrid hollow spheres

Raman-active nanoparticles, as a class of emerging labels, have been attracting considerable attention due to their application in high-sensitivity bioassays. Traditional methods are based on direct attachment of both the Raman reporter and biomolecule to the nanoparticle probe. However, individual spherical Au nanoparticles, which produced relatively weak Raman signals for small organic compounds as labels, were employed. According to theoretical calculations, a molecule at the junction between aggregated nanoparticles can produce

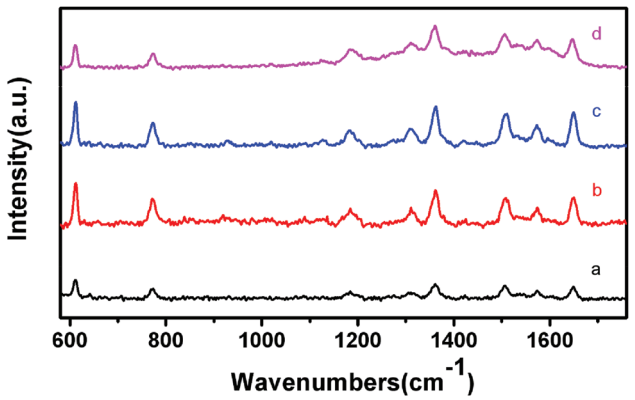

Fig. 5 Raman spectra of R6G (10^{-6} M) adsorbed on Au–Fe_3O_4 hybrid hollow spheres prepared with various Au/Fe molar ratios: (a) Au–Fe_3O_4-0.05, (b) Au–Fe_3O_4-0.1, (c) Au–Fe_3O_4-0.2 and (d) Au–Fe_3O_4-0.5.

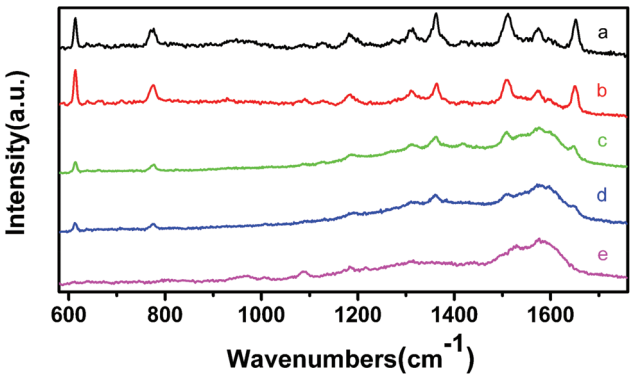

Fig. 6 Raman spectra of R6G with different concentrations adsorbed on Au–Fe_3O_4-0.2 hybrid hollow spheres: (a) 10^{-6} M, (b) 10^{-7} M, (c) 10^{-8} M, (d) 10^{-9} M, and (e) 10^{-10} M.

Raman scattering intensity several orders of magnitude higher than a molecule on the surface of a single spherical nanoparticle.[39] Thus, it would be interesting to explore whether the as-prepared hybrid magnetic hollow spheres could be used for fabricating substrates for intense SERS. Fig. 5 depicts the SERS spectrum of R6G (10^{-6} M) adsorbed on the surface of hybrid hollow spheres prepared at different Au/Fe molar ratios. It is found that all the four hybrid hollow spheres have superior SERS sensitivity to R6G molecules. The peaks from 600 to 1700 cm^{-1} are attributed to R6G signals. Vibrations at 1183, 1311, 1363, 1509, and 1651 cm^{-1} are assigned to C–H in-plane bending, C–O–C stretching, and C–C stretching of the aromatic ring,[40] and a low concentration of R6G produces a clear enhanced effect at 1651 cm^{-1}, which is one of the main characteristic bands.[41] The peak at 772 cm^{-1} is due to the out-of-plane bending motion of the hydrogen atoms of the xanthene skeleton.[42] It is clearly seen that with the increase of the Au weight ratio, the SERS signal intensity enhanced first and then weakened. This phenomenon can be explained by the following factors. First, the large weight ratio of Au located in the hybrid hollow spheres can endow increased hot spots and provide a significant Raman enhancement through EM field enhancements. Second, the samples possessing a high specific surface area can favor the adsorption of the probe molecules, but with the increase of weight ratio of Au nanoparticles located in the hollow spheres, the value of the surface area decreases, which is not favorable for the adsorption of the probe molecules. Third, these ordered magnetic samples obtained by an external magnetic field can provide more active sites which afford abundant potential "hot spots" to amplify the local electromagnetic fields as well as the Raman signal. When excited by the incident radiation, a collective surface plasmon is trapped between the neighboring nanoscale gaps, thus creating a huge local electric field at these gaps.[40] However, with the increase of the Au weight ratio in the hollow hybrids, the coercivity shows a clear increase, which would have an impairing influence on SERS due to a widening of the energy gap for charge transfer and a decrease of the electrons on the metal surface.[43] At the beginning, with the increase of the Au weight ratio, the first factor plays a key role, so the SERS signal intensity enhances. When the molar ratio of Au/Fe is larger than 0.2, the other two factors become dominant, so the SERS signal intensity weakens. Thus the sample of Au–Fe_3O_4-0.2 exhibits the highest enhancement efficiency.

Subsequently, a series of SERS spectra were performed for R6G by varying its concentration from 10^{-6} to 10^{-10} M. It can be observed that the sample of Au–Fe_3O_4-0.2 significantly reduces the detection limit of R6G adsorbed on the optimum procedure-prepared hybrid substrate, as shown in Fig. 6. The spectral intensities and resolutions are decreased by diluting the concentration of the target molecule and the peak at about 1509 and 1651 cm^{-1} can be observed clearly even at 10^{-10} M. These results demonstrate that the Au–Fe_3O_4-0.2 hybrid hollow spheres have a good detection limit as an SERS template. Thus, the hybrids could be applicable for the trace detection of pollutants or other biomolecular species, and this remains to be investigated.

3.3. Catalytic properties of the Au–Fe_3O_4 hybrid hollow spheres

With high specific surface area, functional and tunable shell and magnetic properties, as-prepared hollow spheres are expected to be widely applied in magnetic separable nanocatalysts. In order to investigate the catalytic performance of the Au–Fe_3O_4 hybrid hollow spheres, the reduction of 4-NP by $NaBH_4$ is chosen as a model reaction. For the reduction process of 4-NP, the extent of the reaction could be determined by measuring the change of the absorbance at 400 nm. Fig. 7a shows the typical UV-visible absorption spectra of 4-NP catalyzed by the Au–Fe_3O_4-0.2 hybrid hollow spheres with an appropriate Au weight ratio. After adding the Au–Fe_3O_4 hybrid spheres, the peak intensity at 400 nm decreases with a concomitant increase in peaks of 4-aminophenol (4-AP) at 230 and 300 nm. The disappearance of the peak at 400 nm indicates the completion of the reaction within 3 min. And the color of the mixture gradually changes from yellow to colorless.

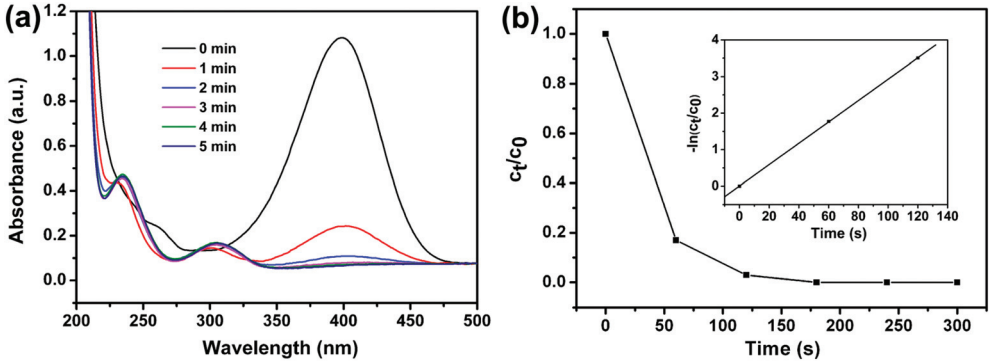

Fig. 7 (a) UV/Vis absorption spectrum of 4-NP catalyzed by the Au–Fe_3O_4-0.2 hybrid hollow spheres and (b) concentration change in 4-NP (C_t/C_0) in the presence of Au–Fe_3O_4-0.2 hybrid hollow spheres. Inset in (b) is the linear relationship of $\ln(C_t/C_0)$ as a function of time for 4-NP.

In light of the much higher concentration of $NaBH_4$ than 4-NP, the pseudo-first-order kinetics can be applied to evaluate the catalytic activity of the Au–Fe_3O_4 hybrid spheres. The concentration of 4-NP at time t is denoted C_t, and the initial concentration of 4-NP at $t = 0$ is regarded as C_0. The ratio of C_t to C_0 is measured from the relative intensity of absorbance (A_t/A_0). The linear relationship of $\ln(C_t/C_0)$ *versus* time (t) indicates that the reduction of 4-NP by the Au–Fe_3O_4 hybrid spheres follows the pseudo-first-order kinetics (Fig. 7b). The rate constant (k) is calculated to be 1.76 min^{-1} from the slope, which is higher than the previously reported values obtained from the same catalytic reaction using different Au-based materials (Table S1†).[28,44] This result clearly indicates that Au–Fe_3O_4 hybrid hollow spheres are superior nanocatalysts which can enhance the catalytic efficiency and minimize the used amounts of catalysts for the reaction. As practical catalysts, reusability, recoverability, and high catalytic activity in each cycle are necessary. The Au–Fe_3O_4 hybrid hollow spheres can be easily recycled by an external magnet after the catalytic reduction. Fig. 8 shows the magnetically recyclable reduction of 4-NP in the presence of Au–Fe_3O_4-0.2 nanocatalysts. The catalysts can be successfully recycled and reused for at least six successive cycles of reaction with a stable conversion efficiency of around 100%. Through the above analysis, it is concluded that the Au–Fe_3O_4 hybrids have excellent catalytic activity for the reduction of 4-NP, which may be attributed to the synergistic effect between Au and Fe_3O_4 nanoparticles. As for the one-pot solvothermal process, the epitaxial growth of Fe_3O_4 on Au ensures efficient partial electron transfer between Au and Fe_3O_4 nanoparticles. The Fe_3O_4 nanoparticles may serve as an electron storage container, which increases electron availability for the reduction of 4-NP. So the catalytic activity of the Au–Fe_3O_4 hybrid hollow spheres is significantly enhanced.[28] Thus, the as-synthesized Au–Fe_3O_4 hybrid hollow spheres show promise for potential application as recyclable catalysts in waste water treatment.

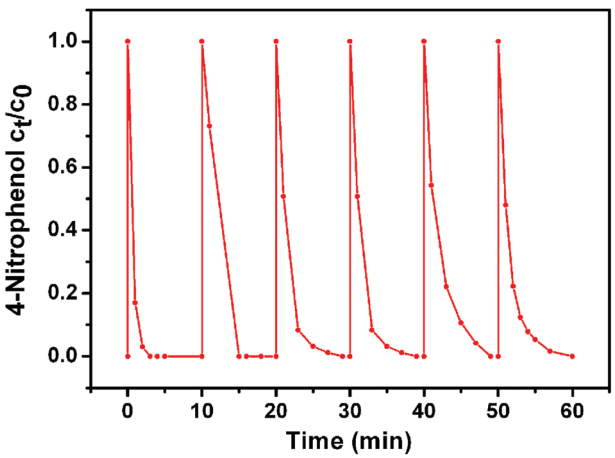

Fig. 8 Catalytically recyclable reduction of 4-NP by the Au–Fe_3O_4-0.2 hybrid hollow spheres in the presence of $NaBH_4$.

4. Conclusions

In summary, we have demonstrated a facile one-pot hydrothermal method for the controlled synthesis of porous Au–Fe_3O_4 hybrid hollow spheres. The amount of Au nanoparticles located in the hybrid hollow spheres can be tuned by changing the molar ratio of Au/Fe precursors. The key structural feature of the as-prepared Au–Fe_3O_4 hybrid hollow spheres is that a strong metal–oxide interaction exists at the interface due to the epitaxial growth of Fe_3O_4 on Au. The SERS study shows that all the four obtained Au–Fe_3O_4 hybrid hollow spheres have superior SERS sensitivity for R6G detection, and the sample of Au–Fe_3O_4-0.2 exhibits the strongest enhancement. The detection limit of the Au–Fe_3O_4-0.2 hybrid hollow spheres for R6G can reach up to 10^{-10} M, which can meet the required concentration level for ultratrace detection of analytes using SERS. In addition, those hybrids can also be used as ideal recyclable catalysts for liquid-phase reactions. The catalytic experiments of the sample of Au–Fe_3O_4-0.2 demonstrate that the model of 4-NP molecules can be degraded within 3 min and the catalytic activity can be recovered without sharp activity loss in six runs, which indicates their superior catalytic degradation activity. The reason for this may be due to the

highly efficient partial charge transfer between Au and Fe_3O_4 at the nanoscale interface. Thus it can be anticipated that the bifunctional Au–Fe_3O_4 hybrid hollow spheres may have great potential in trace detection and industrial waste water treatment. Finally, due to its simplicity and reproducibility, the strategy mentioned here for the production of bifunctional hybrid materials can be readily scaled up.

Acknowledgements

This work was supported by the National Natural Science Foundation of China (no. 61378038, 21301179), the National Basic Research Program of China (2011CB302103) and the China Postdoctoral Special Science Foundation (2012M511430). We also acknowledge the support of the State Key Laboratories of Transducer Technology.

References

1 J. H. Gao, G. L. Liang, B. Zhang, Y. Kuang, X. X. Zhang and B. Xu, *J. Am. Chem. Soc.*, 2007, **129**(5), 1428–1433.
2 E. V. Shevchenko, M. I. Bodnarchuk, M. V. Kovalenko, D. V. Talapin, R. K. Smith, S. Aloni, W. Heiss and A. P. Alivisatos, *Adv. Mater.*, 2008, **20**(22), 4323.
3 T. Yu, J. Zeng, B. Lim and Y. N. Xia, *Adv. Mater.*, 2010, **22**(45), 5188–5192.
4 I. Thomann, B. A. Pinaud, Z. Chen, B. M. Clemens, T. F. Jaramillo and M. L. Brongersma, *Nano Lett.*, 2011, **11**(8), 3440–3446.
5 J. Bao, W. Chen, T. T. Liu, Y. L. Zhu, P. Y. Jin, L. Y. Wang, J. F. Liu, Y. G. Wei and Y. D. Li, *ACS Nano*, 2007, **1**(4), 293–298.
6 R. G. Chaudhuri and S. Paria, *Chem. Rev.*, 2012, **112**(4), 2373–2433.
7 X. L. Zhao, Y. Q. Cai, T. Wang, Y. L. Shi and G. B. Jiang, *Anal. Chem.*, 2008, **80**(23), 9091–9096.
8 C. J. Xu, J. Xie, D. Ho, C. Wang, N. Kohler, E. G. Walsh, J. R. Morgan, Y. E. Chin and S. H. Sun, *Angew. Chem., Int. Ed.*, 2008, **47**(1), 173–176.
9 C. J. Xu, B. D. Wang and S. H. Sun, *J. Am. Chem. Soc.*, 2009, **131**(12), 4216–4217.
10 H. Y. Xie, R. Zhen, B. Wang, Y. J. Feng, P. Chen and J. Hao, *J. Phys. Chem. C*, 2010, **114**(11), 4825–4830.
11 Y. Liu, C. J. Jia, J. Yamasaki, O. Terasaki and F. Schüth, *Angew. Chem., Int. Ed.*, 2010, **49**(33), 5771–5775.
12 C. S. Levin, C. Hofmann, T. A. Ali, A. T. Kelly, E. Morosan, P. Nordlander, K. H. Whitmire and N. J. Halas, *ACS Nano*, 2009, **3**(6), 1379–1388.
13 Z. C. Xu, Y. L. Hou and S. H. Sun, *J. Am. Chem. Soc.*, 2007, **129**(28), 8698–8699.
14 Y. Wei, R. Klajn, A. O. Pinchuk and B. A. Grzybowski, *Small*, 2008, **4**(10), 1635–1639.
15 L. Y. Wang, J. Luo, Q. Fan, M. Suzuki, I. S. Suzuki, M. H. Engelhard, Y. H. Lin, N. Kim, J. Q. Wang and C. J. Zhong, *J. Phys. Chem. B*, 2005, **109**(46), 21593–21601.
16 H. Yu, M. Chen, P. M. Rice, S. X. Wang, R. L. White and S. H. Sun, *Nano Lett.*, 2005, **5**(2), 379–382.
17 W. Wu, Q. G. He, H. Chen, J. X. Tang and L. B. Nie, *Nanotechnology*, 2007, **18**(14), 145609.
18 S. J. Guo, S. J. Dong and E. K. Wang, *Chem. – Eur. J.*, 2009, **15**(10), 2416–2424.
19 S. F. Chin, K. S. Iyer and C. L. Raston, *Cryst. Growth Des.*, 2009, **9**(6), 2685–2689.
20 I. Y. Goon, L. M. H. Lai, M. Lim, P. Munroe, J. J. Gooding and R. Amal, *Chem. Mater.*, 2009, **21**(4), 673–681.
21 F. Bao, J. L. Yao and R. A. Gu, *Langmuir*, 2009, **25**(18), 10782–10787.
22 J. Zhang, X. H. Liu, X. Z. Guo, S. H. Wu and S. R. Wang, *Chem. – Eur. J.*, 2010, **16**(27), 8108–8116.
23 Q. Zhang, J. P. Ge, J. Goebl, Y. X. Hu, Y. G. Sun and Y. D. Yin, *Adv. Mater.*, 2010, **22**(17), 1905–1909.
24 Y. Wang, Y. H. Shen, A. J. Xie, S. K. Li, X. F. Wang and Y. Cai, *J. Phys. Chem. C*, 2010, **114**(10), 4297–4301.
25 Z. H. Xu, C. X. Li, X. J. Kang, D. M. Yang, P. P. Yang, Z. Y. Hou and J. Lin, *J. Phys. Chem. C*, 2010, **114**(39), 16343–16350.
26 H. L. Liu, J. H. Wu, J. H. Min and Y. K. Kimc, *J. Alloys Compd.*, 2012, **537**, 60–64.
27 H. Wang, Y. B. Sun, Y. F. Yu, J. Chen, R. Li, K. Cheng and Q. W. Chen, *Dalton Trans.*, 2012, **41**(2), 346–350.
28 X. W. Meng, B. Li, X. L. Ren, L. F. Tan, Z. B. Huang and F. Q. Tang, *J. Mater. Chem. A*, 2013, **1**(48), 10513–10517.
29 A. Mezni, I. Balti, A. Mlayah, N. Jouini and L. S. Smiri, *J. Phys. Chem. C*, 2013, **117**(31), 16166–16174.
30 (*a*) Y. J. Xiong, J. M. McLellan, Y. D. Yin and Y. N. Xia, *Angew. Chem., Int. Ed.*, 2007, **46**(5), 790–794; (*b*) K. R. Brown, D. G. Walter and M. J. Natan, *Chem. Mater.*, 2000, **12**(2), 306–313; (*c*) M. P. Mallin and C. J. Murphy, *Nano Lett.*, 2002, **2**(11), 1235–1237.
31 A. N. Pham and T. D. Waite, *J. Phys. Chem. A*, 2008, **112**(4), 643–651.
32 Y. Peng, A. W. Xu, B. Deng, M. Antonietti and H. Cölfen, *J. Phys. Chem. B*, 2006, **110**(7), 2988–2993.
33 G. Z. Wang, R. Saeterli, P. M. Rorvik, A. T. J. van Helvoort, R. Holmestad, T. Grande and M. A. Einarsrud, *Chem. Mater.*, 2007, **19**(9), 2213–2221.
34 Z. M. Cui, L. Y. Jiang, W. G. Song and Y. G. Guo, *Chem. Mater.*, 2009, **21**(6), 1162–1166.
35 J. G. Yu, J. C. Yu, W. K. Ho, M. K. P. Leung, B. Cheng, G. K. Zhang and X. J. Zhao, *Appl. Catal., A*, 2003, **255**(2), 309–320.
36 L. P. Zhu, H. M. Xiao, W. D. Zhang, G. Yang and S. Y. Fu, *Cryst. Growth Des.*, 2008, **8**(3), 957–963.
37 S. Peng, C. H. Lei, Y. Ren, R. E. Cook and Y. G. Sun, *Angew. Chem., Int. Ed.*, 2011, **50**(14), 3158–3163.
38 A. K. Boal, B. L. Frankamp, O. Uzun, M. T. Tuominen and V. M. Rotello, *Chem. Mater.*, 2004, **16**(17), 3252–3256.
39 C. Wang, Y. Chen, T. Wang, Z. Ma and Z. Su, *Adv. Funct. Mater.*, 2008, **18**(2), 355–361.

40 Q. Gao, A. W. Zhao, Z. B. Gan, W. Y. Tao, D. Li, M. F. Zhang, H. Y. Guo, D. P. Wang, H. H. Sun, R. R. Mao and E. H. Liu, *CrystEngComm*, 2012, **14**(24), 4834–4842.
41 P. Hildebrandt and M. Stockburger, *J. Phys. Chem.*, 1984, **88**(24), 5935–5944.
42 H. X. Xu, E. J. Bjerneld, M. Kăll and L. Bŏrjesson, *Phys. Rev. Lett.*, 1999, **83**(21), 4357–4360.
43 X. K. Kong, Q. W. Chen, R. Li, K. Cheng, N. Yan and B. X. Yu, *Chem. Commun.*, 2011, **47**(40), 11237–11239.
44 M. H. Rashid, R. R. Bhattacharjee, A. Kotal and T. K. Mandal, *Langmuir*, 2006, **22**(17), 7141–7143.